Oxygen interaction with disordered and nanostructured Ag(001) surfaces

L. Vattuone,[a] U. Burghaus,[b] L. Savio, M. Rocca, G. Costantini,[c] F. Buatier de Mongeot, C. Boragno, S. Rusponi,[d] and U. Valbusa
Centro di Fisica delle Superfici e delle Basse Temperature del C.N.R, Istituto Nazionale per la Fisica della Materia, and Dipartimento di Fisica, via Dodecaneso 33, 16146 Genova, Italy

(Received 19 March 2001; accepted 25 May 2001)

We investigated O_2 adsorption on Ag(001) in the presence of defects induced by Ne^+ sputtering at different crystal temperatures, corresponding to different surface morphologies recently identified by scanning tunneling microscopy. The gas-phase molecules were dosed with a supersonic molecular beam. The total sticking coefficient and the total uptake were measured with the retarded reflector method, while the adsorption products were characterized by high resolution electron energy loss spectroscopy. We find that, for the sputtered surfaces, both sticking probability and total O_2 uptake decrease. Molecular adsorption takes place also for heavily damaged surfaces but, contrary to the flat surface case, dissociation occurs already at a crystal temperature, T, of 105 K. The internal vibrational frequency of the O_2 admolecules indicates that two out of the three O_2^- moieties present on the flat Ag(001) surface are destabilized by the presence of defects. The dissociation probability depends on surface morphology and drops for sputtering temperatures larger than 350 K, i.e., when surface mobility prevails healing the defects. The latter, previously identified with kink sites, are saturated at large O_2 doses. The vibrational frequency of the oxygen adatoms, produced by low temperature dissociation, indicates the formation of at least two different adatom moieties, which we tentatively assign to oxygen atoms at kinks and vacancies. © *2001 American Institute of Physics.* [DOI: 10.1063/1.1386432]

I. INTRODUCTION

One ultimate goal of catalysis is the design of catalysts characterized by a well-defined reactivity and selectivity for a chemical reaction. To achieve this goal an understanding of the influence of the geometric and electronic structure of catalysts on the reactivity is necessary.[1–3] A number of different approaches to attack this problem have been conducted, as, e.g., atomic-scale fabrication of novel surfaces[4] by the tip of a scanning tunneling microscope. A more simple way to contribute to this research topic is to modify the structure of a standard catalyst by sputtering, and to investigate first the adsorption of molecules which might dissociate preferentially at defect sites[5] and subsequently bimolecular reactions. An increase of the product formation rates caused by the defects of the catalyst, produced by a pulsed laser, has indeed been observed for CO oxidation on Pt(111).[6] The higher catalytic activity was attributed to the increased sticking probability of oxygen. An enhanced reactivity was also observed for water formation on stepped Ru(001).[7] For CO oxidation on Pt(112), on the contrary, a reduced reactivity was reported for step sites as compared to terrace sites.[8,9] Thus, a detailed understanding of the kinetics and dynamics of the dissociation of molecules in the presence of defects is extremely important, since this process is frequently the rate determining step in chemical reactions.[10–13]

Recently some of us (S.R., C.B., and U.V.)[14] demonstrated by scanning tunneling microscopy (STM) that the morphology of surfaces can be changed *in situ* by Ar bombardment because of the interplay between the sputtering action of Ar ions and the surface mobility. This process leads to the formation of tiny (10-Å-diameter) holes when sputtering is performed at crystal temperature below 180 K and to large corrugations when it takes place near room temperature. When sputtering the surface at normal incidence, the nanostructuring takes the form of ripples for Ag(110)[14] and of a checkerboard structure of pits for Ag(001).[15,16] This crystal face is particularly interesting with respect to chemical reactivity as on the flat surface O_2 adsorption takes place only molecularly at a crystal temperature $T=105$ K.[5,17] In the presence of the checkerboard structure, by contrast, dissociation already occurs at 105 K and the dissociation probability, P_{diss}, can be traced down to the density of kink sites.[18] In the present paper we shall present a more detailed analysis of the spectroscopic data, parametric in sputtering temperature, T_{sput}, oxygen exposure, χ_{O_2}, and ion dose, χ_{Ne^+}.

II. EXPERIMENT

The adsorption experiments were performed in a combined high resolution electron energy loss spectroscopy (HREELS) and supersonic molecular beam apparatus which was described in detail in Ref. 19. Oxygen was dosed with a supersonic molecular beam. The sticking coefficient and total

[a]Author to whom all correspondence should be addressed, electronic mail: vattuone@fisica.unige.it
[b]Present address: Dept. of Chemistry, Ruhr University - Bochum, Germany.
[c]Present address: Max-Planck-Institut fur Festkurperforschung, Heisenbergstr. 1, D-70569 Stuttgar, Germany.
[d]Institut de Physique Exprimentale, Ecole Polytechnique Federale de Lausanne, CH-1015 Lausanne, Switzerland.

uptake were investigated by the retarded reflector method [the King and Wells method (KW)],[20] while the adsorption products were characterized by high resolution vibrational electron energy loss spectroscopy (HREELS). The surface morphology was investigated in a different apparatus with Scanning Tunneling Microscopy (STM).

The silver surface was cleaned by Ne^+ sputtering (1000 eV, 1 μA for 10 min) and annealing to about 740 K. Crystallographic order and cleanliness of the surface were checked by Low Energy Electron diffraction (LEED) and HREELS for the adsorption experiments. The crystal temperature was varied by irradiation and electron bombardment of the back of the crystal and by fluxing liquid nitrogen through a cryostat.

In order to obtain the nanostructuring, in the present experiment the surface was bombarded at normal incidence with 1 keV Ne^+ ions and a current on the sample of 1.2 μA at different T_{sput}. The same experiment was also performed at a grazing sputtering angle, $\theta_{sput}=70°$, with the Ne^+ beam impinging along the $\langle 100\rangle$ direction. Such a direction is chosen as the ripples forming after sputtering at the appropriate temperature exhibit steps with a high kink density.

The Ne pressure was adjusted to keep the Ne^+ flux constant. The choice of Ne^+ as sputter gas instead of Ar^+, as in Ref. 14, is dictated by the lower achieved contamination level as a liquid N_2 trap can be operated while sputtering. STM measurements revealed that the surface morphology obtained by Ne^+ bombardment is the same as with Ar^+ provided that, while using Ne^+, the sputtering dose is corrected for the smaller sputtering yield. The adsorption experiments were performed for χ_{Ne^+} up to 13.5 ML, which corresponds to the condition investigated thoroughly in Ref. 15. Sputtering at room temperature leads to a well-developed checkerboard superstructure.

After each sputtering treatment at a given T_{sput}, the sample was cooled down reaching in a few minutes temperatures below 130 K, thus freezing in the nonequilibrium surface shape. Dioxygen was dosed with the supersonic beam seeded in He (3% O_2) impinging on the surface at normal incidence in order to achieve a large sticking coefficient, S.[21] The experiments were performed at two different values of the translational energies E_i: 0.4 eV (nozzle at room temperature) and 0.8 eV (nozzle at 600 K), the latter corresponding to the maximum value of $S(E_i)$.[21] The retarded reflector measurements were recorded by a quadrupole mass spectrometer not in line of sight with the sample. The uptake was determined by integration of the KW curve after careful calibration of the beam flux by a spinning rotor gauge. The O_2 flux is 0.2 ML/s with the nozzle at room temperature.

The HREEL spectra were recorded in-specular, at an angle of incidence, θ_e, of 63° and with an electron energy of $E_e=1.7$ eV. The elastic count rate in the specular beam decreased with increasing Ne^+ exposure from $\approx 10^5$ cps (flat surface limit) to $\approx 10^3$ cps at $\chi_{Ne^+}\approx 1$ ML, thereby indicating that a substantial defect concentration builds up already at a moderate sputtering dose. This result is consistent with the large sputter yield reported for silver.[22] In order to obtain a sufficient count rate the energy resolution had to be reduced to about 7–9 meV. Above $\chi_{Ne^+}=1$ ML the intensity of the specular peak remained approximately constant.

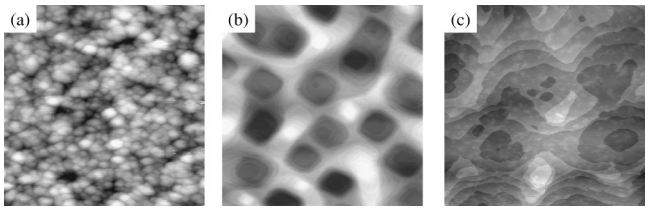

FIG. 1. STM images recorded for different T_{sput} after sputtering the Ag(001) surface by means of 1 keV Ne^+ ions at a flux of 2.1 $\mu A/cm^2$ for 1200 s. (a) 180 K, image size 85×85 nm^2; (b) 380 K, image size 340×340 nm^2; (c) 450 K, image size 700×700 nm^2. Immediately after sputtering the surface is cooled down to below 130 K to freeze in the morphology, a STM image is then acquired.

III. RESULTS

STM images recorded after sputtering at different T_{sput} are shown in Fig. 1. Below $T_{sput}=180$ K the surface is quite rough and the atomic structure cannot be resolved by STM. The local morphology consists of randomly oriented steps, Ag adatoms, and vacancies [see Fig. 1(a)]. With increasing T_{sput} surface mobility sets in and the checkerboard structure develops, consisting of pyramidal pits with ordered (001) terraces and straight $\langle 110\rangle$ steps [see Fig. 1(b)]. Above 400 K the surface becomes smoother, though still not perfectly flat.

Retarded reflector measurements were recorded for the Ag(001) surface sputtered with $\chi_{Ne^+}=13.5$ ML for different T_{sput} and E_i. In Fig. 2 the total sticking probability, S, is plotted in the left-hand panels versus the total (molecular plus atomic) oxygen coverage, Θ (in ML of molecules). As we will demonstrate later, contrary to the flat surface case, partial dissociation takes place here also when dosing O_2 at $T_{ads}=105$ K. The total O_2 uptake, reported in the right-hand panels, was obtained by integration of S with respect to the O_2 flux. In Fig. 3 we report the corresponding curves for $T_{sput}=105$ K parametric in χ_{Ne^+}.

The main result is that both the total sticking probability and the total uptake diminish with decreasing T_{sput} for both E_i values. The decrease of S is about 30% at $T_{sput}=105$ K. Moreover it is apparent that

(a) the sticking probability and the total uptake are reduced with respect to the flat surface limit already at the smallest Ne^+ dose (0.06 ML);
(b) the total sticking probability and the total uptake decrease monotonously with χ_{Ne^+};
(c) S increases with E_i as it did for the flat surface;
(d) The slope of S versus Θ is the same as for the flat surface, indicating that the coverage dependence for the oxygen admolecules is not significantly affected by sputtering.

The information about the fractional coverages of atoms and molecules was determined by vibrational HREELS. The spectra, shown in Fig. 4 parametric in T_{sput}, were recorded for $\chi_{Ne^+}=13.5$ ML and for the small dose $\chi_{O_2}=0.1$ ML at $E_i=0.4$ eV and at an adsorption temperature $T_{ads}=105$ K. The result for the flat surface is shown for comparison, too. Two main losses are present for the damaged surfaces: at

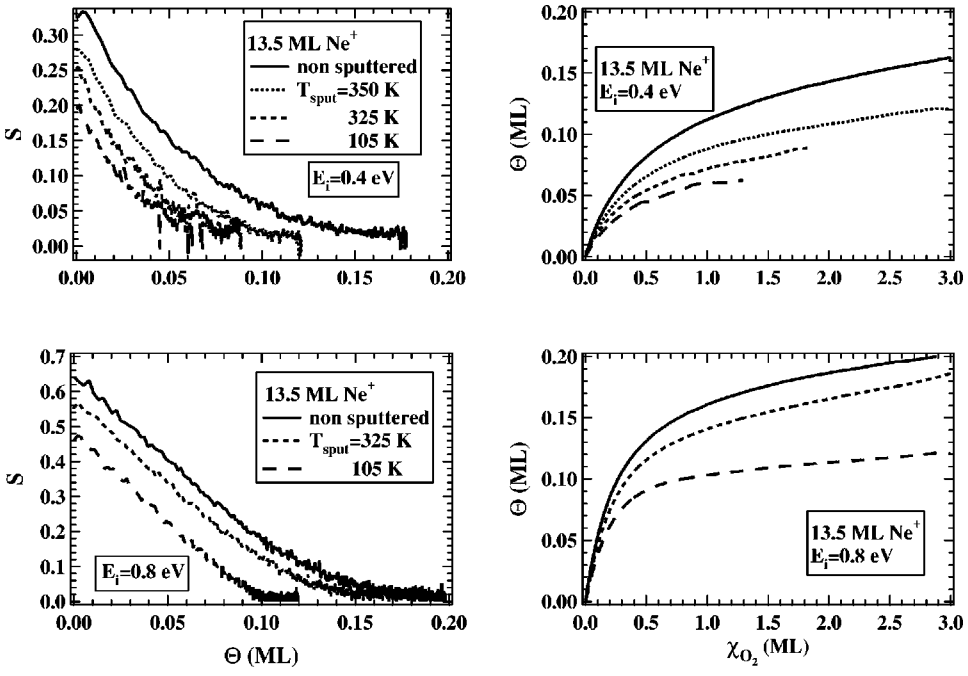

FIG. 2. Dependence of sticking vs coverage and coverage vs exposure for the different surface morphologies obtained at given χ_{Ne^+} vs T_{sput}. Data are presented for impact energies of $E_i = 0.4$ and 0.8 eV.

34–37 meV and at 81 meV. Only one loss, at 81 meV, has significant intensity for the flat surface as well as when T_{sput} is large and the checkerboard structure is washed out.

The latter mode corresponds to the internal vibration of oxygen admolecules,[17,23] which are therefore stable also on such a heavily damaged surface. The intensity of the loss is, however, reduced compared to the flat surface case indicating a smaller molecular oxygen coverage in accord with the retarded reflector measurements.

The losses at 34–37 meV are due to oxygen adatoms whose vibrational energies are in the range from 31 to 36 meV also for flat Ag(001), the exact value depending on oxygen coverage and surface reconstruction.[24] They are therefore indicative that dissociation has taken place for all T_{sput}. A significant contribution of the molecule surface vibration to the energy loss spectra can be excluded as would be expected at 30–32 meV with a much smaller intensity than the mode at 80 meV.[17] This might be the case for the nonsputtered surface, although we are unable to exclude that some dissociation might have occurred also at defects of the nominally flat surface. The presence of impurities, especially of H_2O, OH and CO_3^-, is excluded by measuring HREEL spectra up to loss energies of 500 meV.

By using the total coverage, estimated by the retarded reflector measurements, it is possible to calibrate the intensity of the O–O stretch absolutely for the flat surface case,

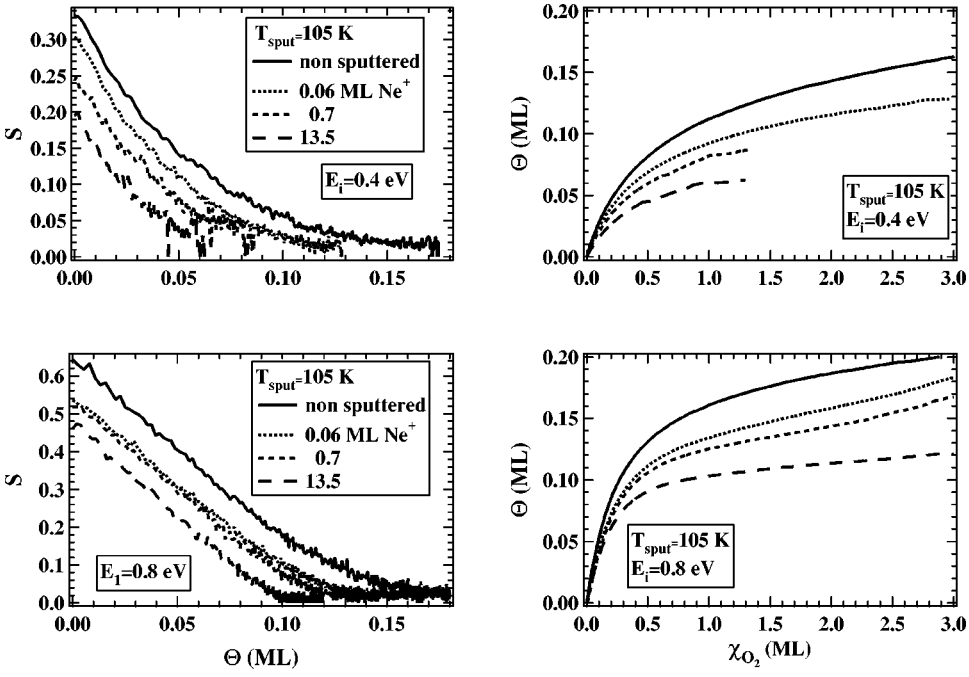

FIG. 3. Dependence of sticking vs coverage and coverage vs exposure for the different surface morphologies obtained at given T_{sput} vs χ_{Ne^+}. Data for $E_i = 0.4$ and 0.8 eV are shown.

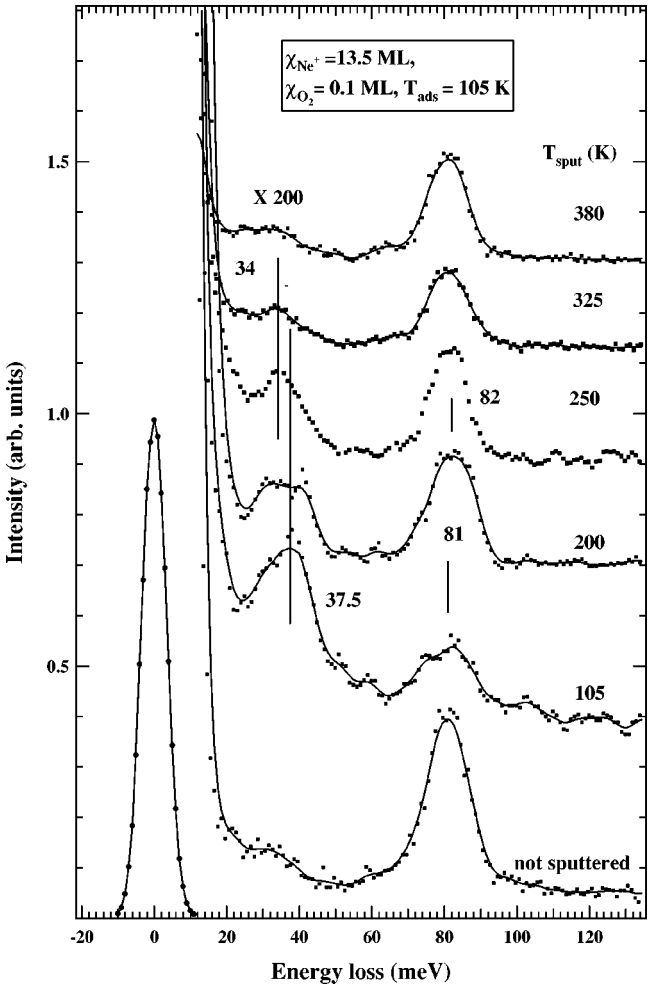

FIG. 4. HREELS spectra recorded after dosing 0.1 ML of O_2 at different T_{sput} and at normal incidence. The losses at 81 meV and 34–37 meV are due to admolecules and adatoms, respectively.

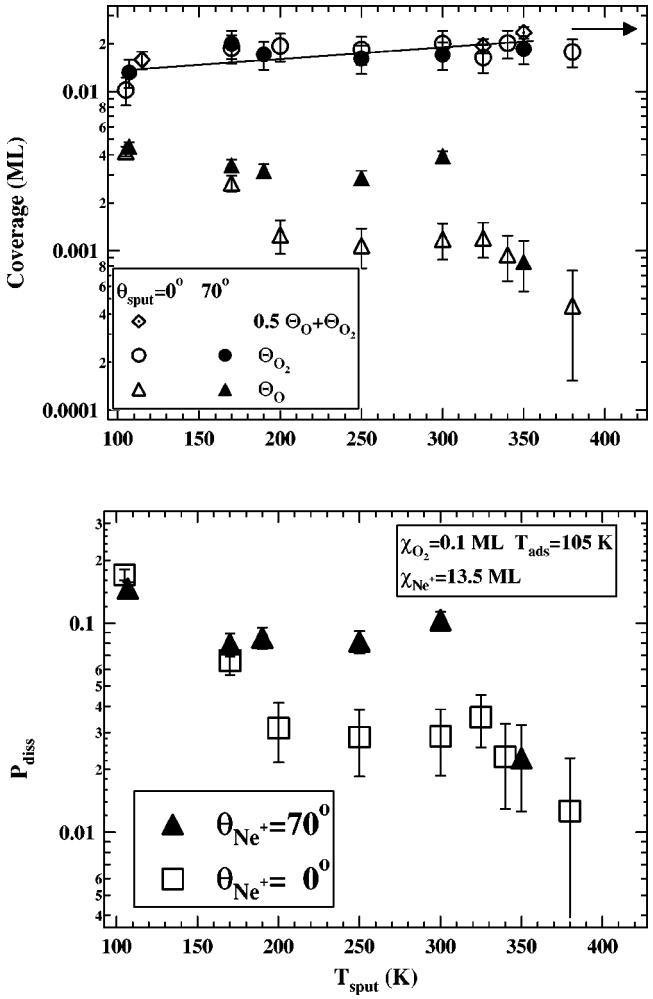

FIG. 5. Coverage of atomic and molecular oxygen and dissociation probability vs sputtering temperature in the low coverage limit for normal and grazing incidence of Ne^+ ions. The arrow indicates the flat surface limit. Θ_{O_2} and Θ_O are in ML of molecules and atoms, respectively. The total coverage (open diamonds) is determined by KW measurements. The line is a guide for the eye, note the increase of the total oxygen coverage with T_{sput}.

where only admolecules are present.[25] Assuming the proportionality factor between loss intensity and absolute coverage as for flat Ag(001), it is possible to estimate the molecular coverage Θ_{O_2}. The atomic coverage, Θ_O, can then be calculated from the difference between the total oxygen uptake and Θ_{O_2}, thus allowing one to determine the dynamic dipole moment and a proportionality factor. The loss intensity is determined by fitting the loss spectrum with a Gaussian curve plus a background; the background is described by a decreasing exponential plus a constant for the losses at energy below 50 meV, where the tail of the elastic peak is nonnegligible, and by a constant alone for higher energy losses. We then define the dissociation probability P_{diss} as

$$P_{diss}=\frac{\Theta_O}{\Theta_O+2\Theta_{O_2}}. \quad (1)$$

The so-determined atomic and molecular oxygen coverages and the calculated dissociation probability are reported in Fig. 5 ($\theta_{sput}=0°$ and 70°) and Fig. 6 ($\theta_{sput}=0°$) versus T_{sput} for two cases corresponding, respectively, to $\chi_{O_2}=0.1$ ML and $\chi_{Ne^+}=13.5$ ML (Fig. 5) and $\chi_{O_2}=0.4$ ML and $\chi_{Ne^+}=2.3$ ML (Fig. 6). The dependence versus χ_{Ne^+} is reported in Fig. 7 for the small oxygen exposure. This analysis shows the following:

(a) For the sputtered surface Θ_{O_2} is smaller than for the flat surface (especially at $T_{sput}=105$ K) and recovers with increasing T_{sput} (Fig. 5, upper panel).

(b) In the T_{sput} range between 180 and 350 K, P_{diss} is more than twice as large when sputtering is performed at grazing angle of incidence rather than at normal incidence (see the lower panel in Fig. 5). This experimental condition corresponds to the formation of ripples along the ⟨100⟩ direction, i.e., to a high density of kinked steps. The difference in P_{diss} between grazing and normal sputtering conditions is small when $T_{sput}<180$ K or >350 K.

(c) P_{diss} is largest for $T_{sput}=105$ K and decreases with T_{sput}, becoming eventually negligible (Fig. 5, lower panel).

(d) The dependence of P_{diss} on T_{sput} for the larger oxygen dose and smaller χ_{Ne^+} (see Fig. 6) is similar to the dependence observed at low oxygen dose, but its values are

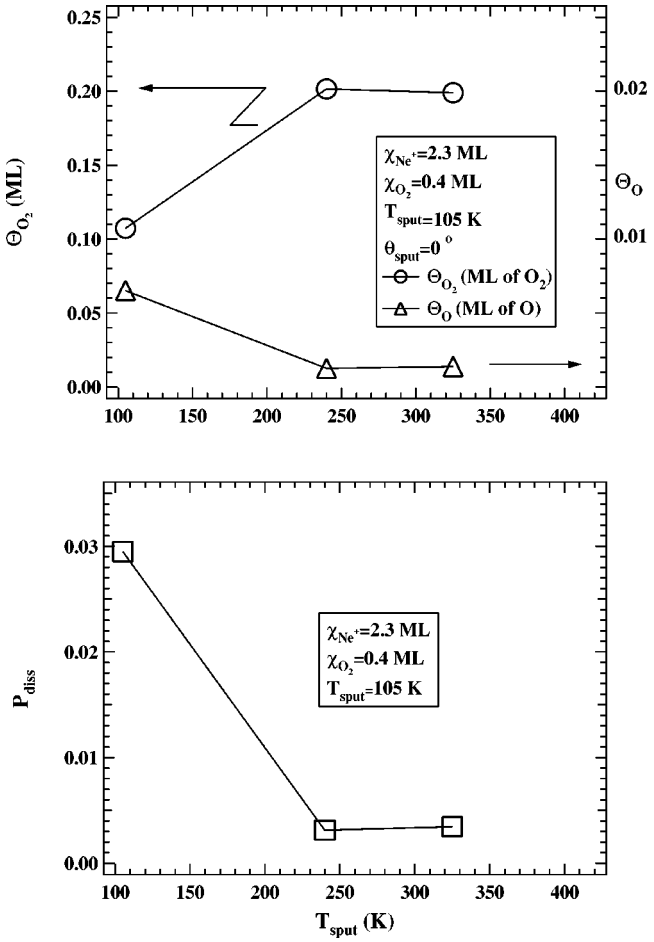

FIG. 6. Coverage of atomic and molecular oxygen and dissociation probability vs sputtering temperature for $\chi_{Ne^+}=2.3$ ML and $\chi_{O_2}=0.4$ ML. The arrows indicate that different scales were used for Θ_O and Θ_{O_2}. The lines are a guide to the eye.

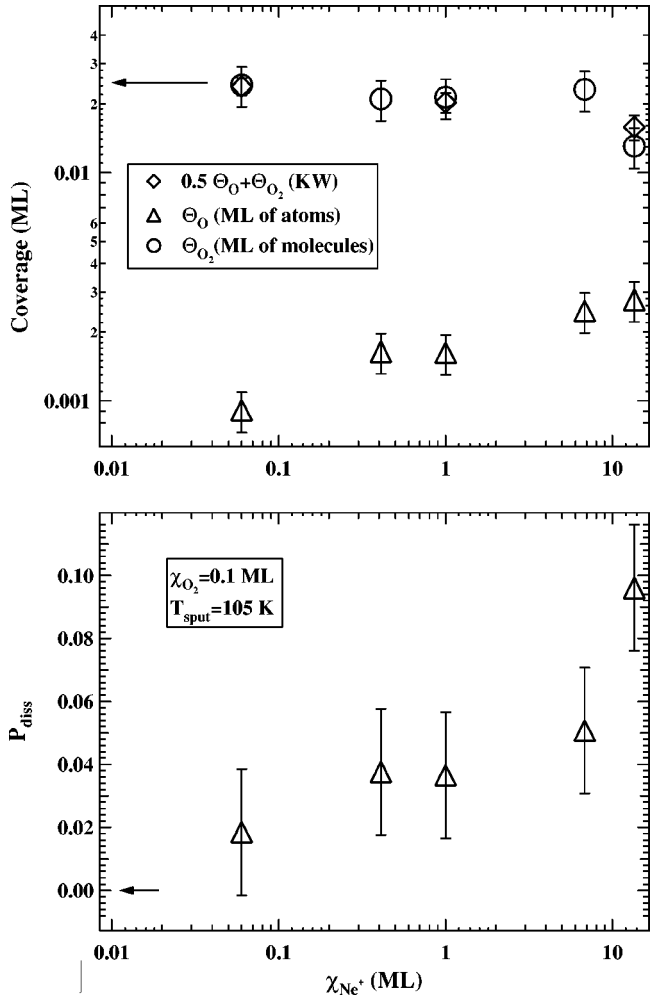

FIG. 7. Coverage of atomic and molecular oxygen and dissociation probability vs Ne^+ dose for $T_{sput}=105$ K, $\chi_{O_2}=0.1$ ML and normal incidence. The arrows indicate the flat surface limit.

substantially smaller. This indicates that after saturation of the defects active for dissociation, occurring in the very early stages of the oxygen exposure, the dynamics of the system is dominated by molecular chemisorption.

(e) P_{diss} increases initially rapidly with χ_{Ne^+} (see Fig. 7: it already reads 0.04 after only 0.5 ML of ions) and grows eventually more slowly reaching 0.10 at the largest χ_{Ne^+}.

Inspection of the HREELS data in Fig. 4 shows moreover that the Ag–O vibrational energy, $\hbar\omega$(Ag−O), decreases with T_{sput} from 37 meV for $T_{sput}=105$ K to 34 meV for $T_{sput}=300$ K, when the checkerboard structure forms. This shift cannot be due to the contribution of the Ag–O_2 stretch, as such mode has a negligible intensity at low coverage. One might, however, object that on a nanostructured surface the dynamical dipole moment might be larger and the loss would become visible already at low coverage: This explanation is, however, unlikely as we observe that the intensity of the loss at 34–37 meV is unaffected by annealing the surface above 150 K, when O_2 desorbs.

In Fig. 8(a) we show another set of HREELS data, recorded for different χ_{Ne^+} at $T_{sput}=105$ K and dosing 0.1 ML of O_2. As one can see the frequency of the atomic oxygen vibration increases monotonously with χ_{Ne^+}, while the frequency of the intermolecular vibration of O_2 has a more complex behavior as it first increases abruptly and then decreases slowly. A similar experiment was performed at the larger dose of 240 ML [see Fig. 8(b)] and shows similar effects except that the atomic oxygen vibration is initially at 33 meV rather than at 35.5 meV. The results for the vibrational energies, $\hbar\omega$, are summarized in Fig. 9. As is apparent the data separate into two families, characterized by $\hbar\omega=32-34$ meV and $\hbar\omega=35.5-37$ meV, respectively. Distinct oxygen moieties are therefore present: one corresponding to oxygen adatoms at adsorption sites induced only by sputtering at 105 K (loss at 35.5–37 meV) and another to adatoms at sites present also for the checkerboard structure (loss at 34 meV). The latter sites are populated after saturating the former.[26]

Also in Fig. 9, we report the dependence of the internal O–O stretch on χ_{Ne^+}. As mentioned previously the frequency of this mode shifts abruptly to larger energy as soon as some defects are present and resumes eventually the flat surface value for large χ_{Ne^+}. This nonmonotonic behavior can be rationalized if one of the two O_2 moieties, present on the flat Ag(001) surface and giving rise to a doublet at 79 and 84 meV,[23] is destabilized. Such modes cannot be resolved in the present experiment and, being approximately of the same

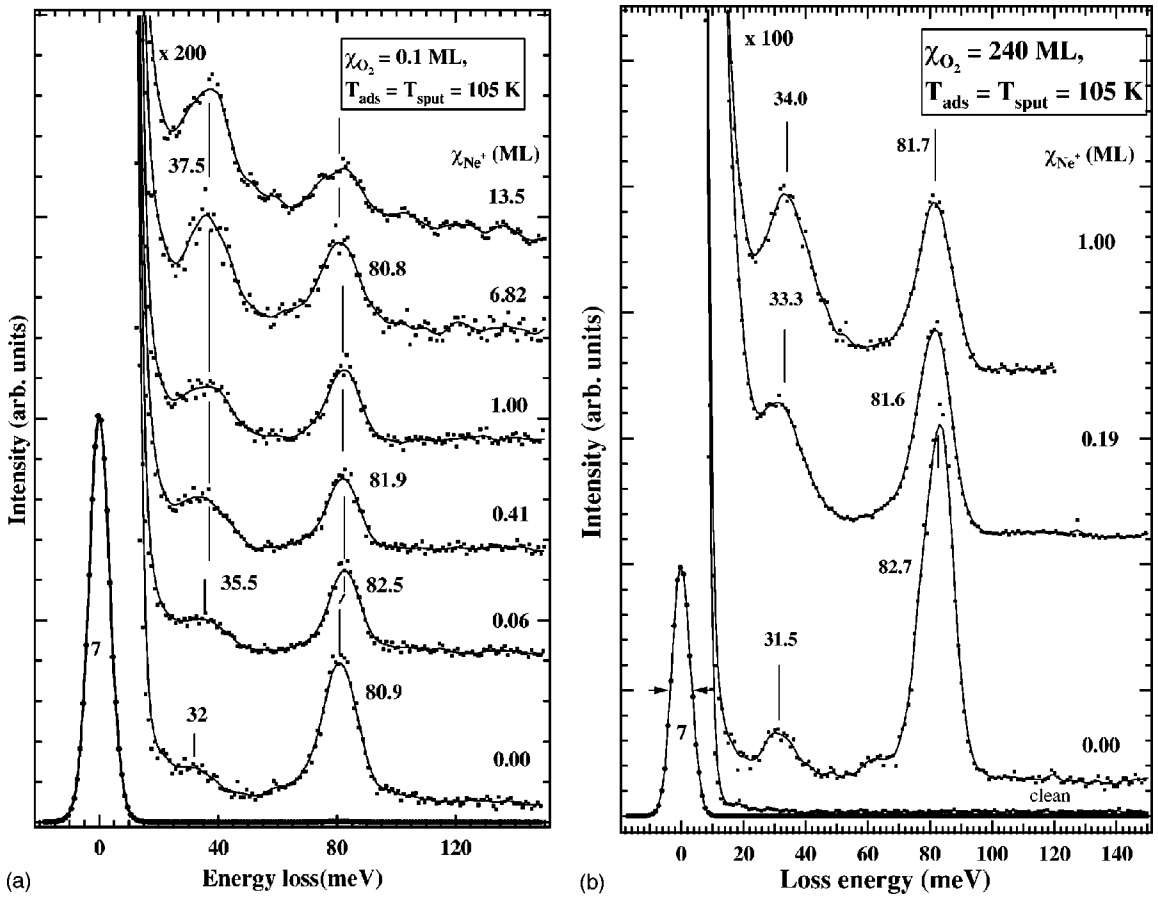

FIG. 8. HREELS spectra for low coverage O_2 adsorption at 105 K, parametric in χ_{Ne^+} for (a) $\chi_{O_2}=0.1$ ML and (b) $\chi_{O_2}=240$ ML.

intensity at low coverage, they give rise to a loss at 81 meV. The maximum of the loss peak would thus shift to higher energy if the ratio of the unresolved peaks changes in favor of the 84 meV loss. The shift to 80 meV occurring at larger χ_{Ne^+} must, on the other hand, have a different reason.

In order to check whether the presence of defects enhances the reactivity of oxygen, CO oxidation was studied. The reaction rate is sensitive to surface geometry, being two orders of magnitude larger for $O_2/Ag(110)$[2,3] than for $O_2/Ag(100)$.[27,28] CO was dosed with the supersonic molecular beam on the O_2 precovered surface. As shown in Fig. 10 (closed symbols) with exposure to CO we observe a decrease in the intensity of the intermolecular vibrational loss peak (at $\approx$80 meV) and an increase of the intensity of the oxygen adatom-substrate vibration (at 35 meV). This indicates CO_2 formation via

$$CO(ad)+O_2(ad)\rightarrow CO_2(gas)+O(ad). \tag{2}$$

The initial reaction probability

$$P_r=\frac{\Delta\Theta_{O_2}}{\chi_{CO}} \tag{3}$$

is, however, approximately equal to the value determined in our prior study for the smooth Ag(001) surface,[28] i.e., $P_r \sim 5\times10^{-4}$ for sputtered and nonsputtered surfaces (open symbols in Fig. 10). The intensity of the oxygen adatom-substrate vibration increases with CO exposure, too, leading to the conclusion that, if removal of atomic oxygen by CO takes place, its rate is smaller than the production through reaction (2), as was the case also for the flat surface. Therefore, presence of defects does not significantly affect the reaction probability for CO oxidation of either O_{ad} or O_{2ad}. The small reaction rate observed on the flat surface is thus not due to the low concentration of defects because otherwise a substantial enhancement of P_{diss} would be observed for the sputtered surface.

IV. DISCUSSION

As anticipated in our previous report[18] the interplay between the morphological information provided by STM images and the quantitative data regarding the chemical properties of the nanostructured surface allows us to trace a correlation between the density of kinks, ρ_{kink}, on the surface and the dissociation probability.

Although highly desirable, an evaluation of the kink density obtained by directly counting the kink sites on high resolution STM images is not practicable because of the high roughness of the sputtered surface. Therefore it is necessary to extract ρ_{kink} from a model of the surface morphology which depends on coarser parameters such as the surface roughness, W, and the mean nanostructures separation, Λ. As already shown in Ref. 18, the surface morphology of sputtered Ag(001) strongly depends on the incidence angle of the

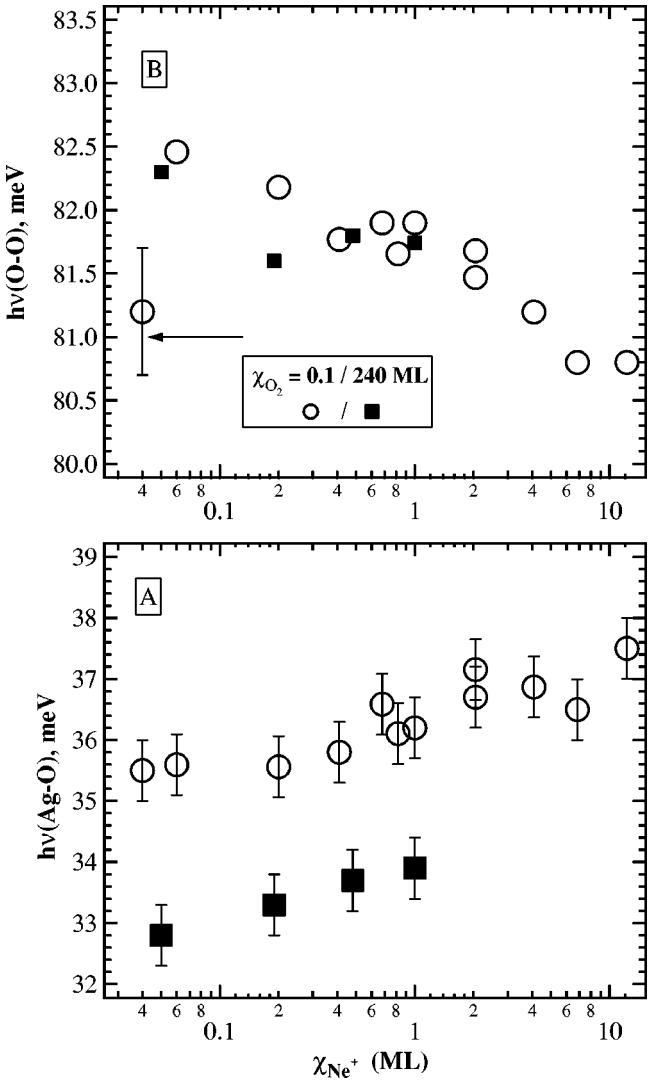

FIG. 9. Electron energy loss data vs Ne^+ exposure, parametric in oxygen exposure. The arrow indicates the low coverage limit on the flat surface for the loss peak associated with the internal stretch of O_2.

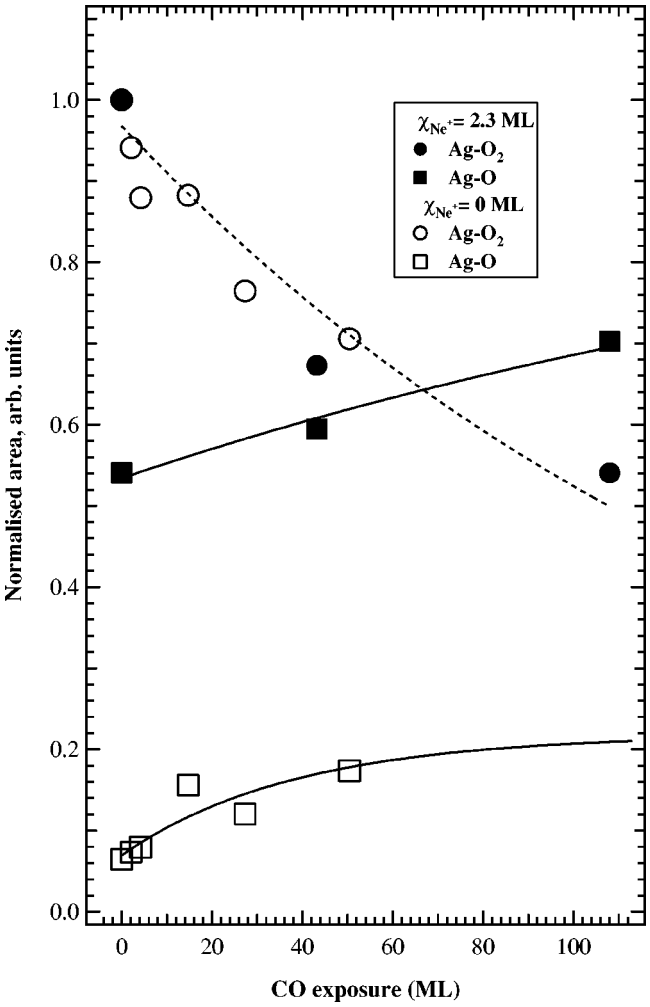

FIG. 10. Influence of defects on the CO oxidation rate by molecularly bonded oxygen at 105 K (closed symbols). The data points show the areas of the loss peaks corresponding to the internal stretching and molecule-surface vibrations normalized to the area of the specular peak which are proportional to the respective coverages. Additionally displayed are the results of the prior study for flat Ag(001) (see Ref. 28, open symbols).

ion, θ_{Ne^+}, resulting in a checkerboard of pits for $\theta_{Ne^+} \approx 0°$, and in a periodic rippled corrugation for $\theta_{Ne^+} \approx 70°$. In the former case, high resolution images of surface morphologies similar to those of Fig. 1(b), show[29] that the straight ⟨110⟩ steps bounding the square pits do not meet at right angles but are connected by rounded corners. These areas are the principal contributors to kink sites, being composed by almost continuous and atomically kinked ⟨100⟩ steps rather than by ⟨110⟩ segments. Therefore ρ_{kink} can be obtained from the total linear extension of these ''rounded corners regions.'' Two other morphological characteristics, resulting from the analysis of a large statistics of STM data, determine our evaluation of the kink site density: (i) independently of T_{sput}, the rounded corners extend over an angle of about 30° from the center of the pits, and (ii) for $T_{sput} \geqslant 380$ K the pits present a flat bottom of width λ [Fig. 11(a)], while at lower temperatures they are stepped over almost all their extension Λ. Putting this information together in a morphological model of the sputtered surface with pyramidal (or truncated pyramidal) pits bounded by rounded corners, we obtain the kink density per atomic site,

$$\rho_{kink} = C_1 \frac{a}{b} \frac{W}{\Lambda} \left[1 - \left(\frac{\lambda}{\Lambda} \right)^2 \right], \tag{4}$$

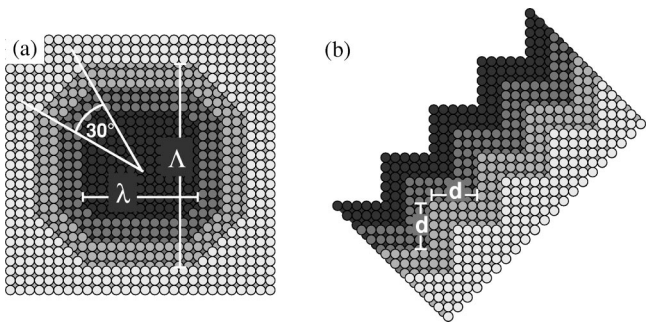

FIG. 11. Morphological model of the sputtered Ag(001) surface; (a) high temperatures and normal ion incidence: a pit with extension Λ and flat bottom λ is shown; (b) low temperatures and grazing ion incidence: saw-toothed shaped side of a ripple.

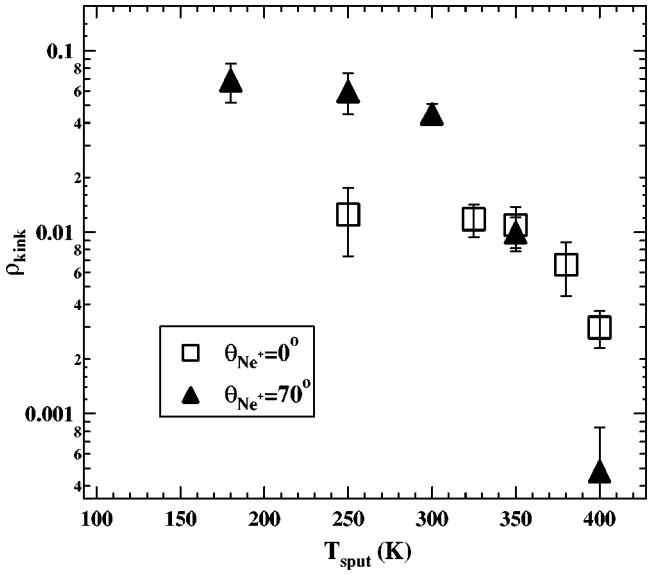

FIG. 12. Density of kinks as obtained by STM vs sputtering temperature.

where $a=2.89$ Å and $b=2.05$ Å are, respectively, the in-plane nearest-neighbor distance and the vertical step height for the Ag(001) surface, W is the surface roughness (the root mean square of the surface fluctuations measured according to Ref. 30), and $C_1 \approx 0.18$ is a numerical factor which derives from the geometrical assumptions of the model.

In the grazing incidence sputtering experiments ($\theta_{Ne^+} \approx 70°$), the ion beam impinges along $\langle 100 \rangle$, i.e., along the diagonal of the surface unit cell. Therefore the ripple structures which form at low temperature are forced to run along a thermodynamically unfavored direction and thus to expose a high number of kinks. Nevertheless high resolution STM images show that the kink sites do not cover the whole sides of the ripples, but are separated by straight $\langle 110 \rangle$ steps with an average extension $d \approx 2$ nm [Fig. 11(b)]; therefore the kink density is equivalent to the step density along the ripple sides divided by d/a. Also in this case, ρ_{kink} can be evaluated by means of a morphological model in which the sputtered surface is approximated by a regular array of infinitely elongated prisms of periodicity Λ (obtained from the mean ripple separation), whose height can be deduced from the surface roughness W. For $T_{sput} > 300$ K, the surface morphology appears similar to the normal sputtering case and therefore the kink density is given by Eq. (4), but for $T < 300$ K it reads

$$\rho_{kink} = C_2 \frac{a^2}{bd} \frac{W}{\Lambda}, \tag{5}$$

where $C_2 \approx 5.64$ is a numerical factor depending on the geometry of the model.

ρ_{kink} is reported in Fig. 12 versus T_{sput} for grazing and normal sputtering conditions. As one can see, below room temperature ρ_{kink} is five times larger for grazing than for normal incidence as in the former case ripples running along the $\langle 001 \rangle$ direction form. In the same temperature range P_{diss} is enhanced by a factor of 4 for grazing incidence (see Fig. 5), indicating thereby a strong correlation with ρ_{kink}. The decrease of both the kink density and the dissociation probability occurs at $T_{sput} > 350$ K.

Adatom-surface vibrations are found at 34 and 37 meV. The lower frequency is observed upon oxygen adsorption at $T=105$ K: (i) on the checkerboard structure for all exposures, and (ii) on the coldly sputtered surface for large O_2 doses. The loss at 37 meV is found, on the contrary, only for oxygen exposures $\chi_{O_2} < 0.5$ ML on surfaces ion bombarded at $T_{sput}=105$ K.

In our previous studies of oxygen adsorption on flat Ag(001), we observed loss energies between 28 and 37 meV depending on the procedure used to dissociate O_2. Adatoms vibrating at 35 meV form upon CO oxidation of O_2/Ag(001),[28] while collision-induced dissociation of O_2/Ag(001) by hyperthermal Xe atoms produces adatoms with stretching frequencies in the range from 28 to 36 meV, depending on impact energy and angle.[31,32] Upon thermal dissociation, adatom species form, vibrating between 30 and 36 meV; the frequency depending on initial coverage and annealing temperature. In particular, the highest value is found for the high coverage, $(2\sqrt{2} \times \sqrt{2})$, missing row reconstructed geometry,[24] in which the oxygen adatoms sit in the former fourfold hollows next to missing $\langle 001 \rangle$ Ag rows.

By comparison with these surfaces, we can thus rationalize our findings on sputtered Ag(001), assigning the two different adatom species to adsorption at vacancies (36–37 meV) and at kinked steps (34–35 meV). The former case suits both to isolated vacancies, present for the coldly sputtered surface, and to the rows of vacancies which build up the $(2\sqrt{2} \times \sqrt{2})$ reconstructed Ag(001). This state therefore corresponds presumably to two oxygen adatoms sitting at opposite corners of the same vacancy and the higher frequency could arise from the stronger dipolar interaction caused by the high local oxygen coverage. The decrease of the oxygen vibration upon large O_2 exposures on the coldly sputtered surface is, on the other hand, indicative that ion bombardment produces a larger concentration of kinked steps than of vacancies and that the former dominate the dissociation process after saturation of the vacancies. A schematic picture of the defect sites is shown in Fig. 12(b).

Upon annealing to 190 K the adatom stretch is at 34 meV, for all sputtered surfaces, indicating either that the isolated vacancies have disappeared and all adatoms now sit at kinks, or that one of the two oxygen atoms in the vacancy has left it.

Let us now discuss the influence of defects on molecularly adsorbed oxygen. The dependence of its internal stretch vibration was reported in Fig. 9 versus χ_{Ne^+} and χ_{O_2}. We notice that the position of the maximum of the loss peak depends little on O_2 dose indicating that the admolecules occupy similar sites at low and large coverages. Moreover we see that the vibrational frequency at low χ_{O_2} and low χ_{Ne^+} (82 meV) is significantly shifted from the flat surface limit of 81 meV (open circles in Fig. 9). The latter peak arises from two distinct contributions, at 79 and 84 meV, corresponding to two different O_2 moieties,[23] which cannot be resolved in the present experiment. The shift of the maxi-

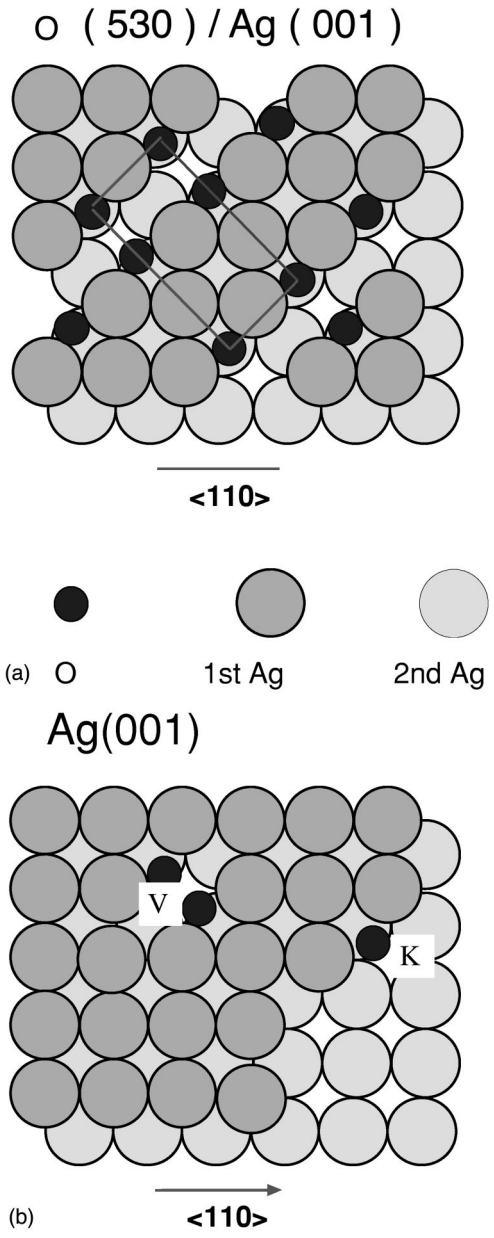

FIG. 13. Schematic drawings (a) of the $(2\sqrt{2}\times\sqrt{2})$ reconstructed phase of O/Ag(001) and (b) of the step and vacancy sites created at low T_{sput}.

mum of the loss peak at low χ_{Ne^+} could thus be due to a change in the ratio of the population of the two moieties caused by sputtering. As the total O_2 uptake is smaller for the damaged surface, the destabilization of the 79 meV moiety must be stronger than the one of the 84 meV species. The 79 meV species corresponds most probably to molecules adsorbed at the fourfold hollows.[23] Its decrease in population could thus reflect the reduced number of nondamaged sites. The 84 meV moiety corresponding to adsorption at bridge sites would be less affected as their concentration is expected to change less with surface damage. The plausibility of this interpretation is further confirmed by the total removal of the 79 meV moiety on Ag(410) where the internal vibration is observed at 85 meV.[33]

With increasing χ_{Ne^+} the loss corresponding to the internal vibration broadens and moves back toward 80 meV indicating either O_2 adsorption at higher coordination sites or an effect associated with coadsorption with atomic oxygen. Finally let us address three intriguing observations.

(i) The global sticking probability and the total uptake decrease with χ_{Ne^+}.

(ii) On the sputtered surface, we were unable to detect the minor loss at about 64 meV, which on flat Ag(001) had been assigned to oxygen molecules adsorbed at defect sites and whose intensity scaled nicely with the coverage dependence of P_{diss}.[5] This finding is probably indicative that such molecules have dissociated already. This conclusion is in accord with the low loss energy which proves a pronounced weakening of the intermolecular bond, which might therefore easily be broken by the interaction with the kink sites. On flat Ag(001) such molecules must therefore sit at defects less reactive than kinks. The higher density of defects on the sputtered surface could therefore lead to dissociation and suppress this loss feature.

(iii) The absence of an effect of sputtering on the reactivity of the O_2 admolecules with CO is surprising, as the CO oxidation reaction is known to be sensitive to surface geometry.[1,28] The only possible explanation for this finding is that although sites with (110) geometry are probably formed with sputtering, the admolecules do not preferentially occupy them.

V. CONCLUSIONS

In conclusion we have shown that contrary to the flat surface case two oxygen adatoms moieties form when adsorption takes place at $T=105$ K on an Ag(001) surface modified by ion bombardment. Molecular adsorption persists also for the most defected surfaces. The dissociation probability can be increased both by lowering the sputtering temperature and by sputtering at grazing incidence along $\langle 100\rangle$. At high oxygen doses when the defects are saturated, dissociation becomes a truly minor channel and molecular chemisorption dominates also for the damaged surface. Morphology affects the adsorption probability also reducing the global O_2 uptake (Fig. 13).

ACKNOWLEDGMENTS

We greatly acknowledge development of a computer controlled electronics for the HREEL spectrometer by G. Maloberti, G. Cicero, and F. Moresco. One of us (U.B.) acknowledges partial financial support from the Deutsche Forschungsgemeinschaft through a postdoctoral fellowship. Professor D. A. King is acknowledged for stimulating discussion. This research was partially financed by the MURST project COFIN 1999.

[1] G. A. Somorjai, Annu. Rev. Phys. Chem. **45**, 721 (1994).
[2] T. Zambelli, J. V. Barth, J. Wintterlin, and G. Ertl, Nature (London) **390**, 495 (1997).
[3] B. Hammer, Phys. Rev. Lett. **83**, 3681 (1999).
[4] K. Tanaka, Y. Okawa, Y. Matsumoto, and T. Fujita, Surf. Sci. **377-379**, 744 (1997).

[5] F. Buatier de Mongeot, A. Cupolillo, U. Valbusa, and M. Rocca, Chem. Phys. Lett. **270**, 345 (1997).
[6] R. Castell, S. Reiff, W. Drachsel, and J. H. Block, Surf. Sci. **377-379**, 770 (1997).
[7] M. H. Koch, P. Jakob, and D. Menzel, Surf. Sci. **367**, 293 (1996).
[8] A. Szabo, M. A. Henderson, and J. T. Yates, J. Chem. Phys. **96**, 6191 (1992).
[9] J. T. Yates, J. Vac. Sci. Technol. A **13**, 1359 (1995).
[10] G. R. Darling and S. Holloway, Rep. Prog. Phys. **58**, 1595 (1995).
[11] R. Imbihl and G. Ertl, Chem. Rev. **95**, 697 (1995).
[12] D. Cappus, C. Xu, D. Ehrlich, B. Dillmann, C. A. Ventrice, Jr., K. Al-Shamery, H. Kuhlenbeck, and H. J. Freund, Chem. Phys. **177**, 533 (1993).
[13] T. Becker, M. Kunat, C. Boas, U. Burghaus, and C. Woll, J. Chem. Phys. **113**, 6334 (2000).
[14] S. Rusponi, C. Boragno, and U. Valbusa, Phys. Rev. Lett. **78**, 2795 (1997).
[15] G. Costantini, S. Rusponi, R. Giannotti, C. Boragno, and U. Valbusa, Surf. Sci. **416**, 245 (1998).
[16] S. Rusponi, G. Costantini, F. Buatier de Mongeot, C. Boragno, and U. Valbusa, Appl. Phys. Lett. **75**, 3318 (1999).
[17] F. Buatier de Mongeot, A. Cupolillo, U. Valbusa, and M. Rocca, J. Chem. Phys. **106**, 9297 (1997).
[18] G. Costantini, F. Buatier de Mongeot, S. Rusponi, C. Boragno, U. Valbusa, L. Vattuone, U. Burghaus, L. Savio, and M. Rocca, J. Chem. Phys. **112**, 6840 (2000).
[19] M. Rocca, U. Valbusa, A. Gussoni, G. Maloberti, and L. Racca, Rev. Sci. Instrum. **62**, 2172 (1991).
[20] D. A. King and M. G. Wells, Surf. Sci. **29**, 454 (1972).
[21] L. Vattuone, U. Burghaus, U. Valbusa, and M. Rocca, Surf. Sci. **408**, L693 (1998).
[22] H. H. Andersen and H. I. Bay, in *Sputtering by Particle Bombardment I*, edited by R. Behrisch (Springer-Verlag, Berlin, 1981).
[23] L. Vattuone, P. Gambardella, U. Valbusa, and M. Rocca, Surf. Sci. **377-379**, 671 (1997).
[24] M. Rocca *et al.*, Phys. Rev. B **61**, 213 (2000).
[25] L. Vattuone, M. Rocca, C. Boragno, and U. Valbusa, J. Chem. Phys. **101**, 713 (1994).
[26] We note that in the case of large O_2 exposure, the weight of the contribution of the molecule–surface stretch increases and might, therefore, cause a shift to lower frequency of the loss attributed to the adatom-surface vibration. The intensity of the former mode is, however, expected to be of, at most, 1/5 of the intensity of the O_2 stretch and its weight is thus negligible.
[27] U. Burghaus and H. Conrad, Surf. Sci. **352-354**, 201 (1996).
[28] U. Burghaus, L. Vattuone, P. Gambardella, and M. Rocca, Surf. Sci. **374**, 1 (1997).
[29] G. Costantini, Ph.D thesis, University of Genova, 2000.
[30] G. Costantini, F. Buatier de Mongeot, C. Boragno, and U. Valbusa, Surf. Sci. **459**, L487 (2000).
[31] L. Vattuone, P. Gambardella, F. Cemic, U. Valbusa, and M. Rocca, Chem. Phys. Lett. **278**, 245 (1997).
[32] L. Vattuone, P. Gambardella, U. Burghaus, F. Cemic, A. Cupolillo, U. Valbusa, and M. Rocca, J. Chem. Phys. **109**, 2490 (1998).
[33] L. Savio, L. Vattuone, and M. Rocca (submitted).